The Meteoritical Society

Meteoritics & Planetary Science 54, Nr 6, 1379–1394 (2019)
doi: 10.1111/maps.13285

Effect of silicon on activity coefficients of Bi, Cd, Sn, and Ag in liquid Fe-Si, and implications for differentiation and core formation

K. RIGHTER [1]*, K. PANDO[2], D. K. ROSS[3], M. RIGHTER[4], and T. J. LAPEN[4]

[1]NASA JSC, Mailcode XI2, 2101 NASA Pkwy, Houston, Texas 77058, USA
[2]UTC–Jacobs JETS Contract, NASA JSC, Houston, Texas 77058, USA
[3]Jacobs-JETS, NASA JSC, University of Texas at El Paso, Houston, Texas 77058, USA
[4]Department of Earth and Atmospheric Sciences, University of Houston, Houston, Texas 77204, USA
*Corresponding author. E-mail: kevin.righter-1@nasa.gov

(Received 20 June 2018; revision accepted 26 February 2019)

Abstract–The depletion of volatile siderophile elements (VSE) Sn, Ag, Bi, Cd, and P in mantles of differentiated planetary bodies can be attributed to volatile-depleted precursor materials (building blocks), fractionation during core formation, fractionation into and retention in sulfide minerals, and/or volatile loss associated with magmatism. Quantitative models to constrain the fractionation due to core formation have not been possible due to the lack of activity and partitioning data. Interaction parameters in Fe-Si liquids have been measured at 1 GPa, 1600 °C and increase in the order Cd (~6), Ag (~10), Sn (~28), Bi (~46), and P (~58). These large and positive values contrast with smaller and negative values in Fe-S liquids indicating that any chalcophile behavior exhibited by these elements will be erased by dissolution of a small amount of Si in the metallic liquid. A newly updated activity model is applied to Earth, Mars, and Vesta. Five elements (P, Zn, Sn, Cd, and In) in Earth's primitive upper mantle can largely be explained by metal-silicate equilibrium at high PT conditions where the core-forming metal is a Fe-Ni-S-Si-C metallic liquid, but two other—Ag and Bi—become overabundant during core formation and require a removal mechanism such as late sulfide segregation. All of the VSE in the mantle of Mars are consistent with core formation in a volatile element depleted body, and do not require any additional processes. Only P and Ag in Vesta's mantle are consistent with combined core formation and volatile-depleted precursors, whereas the rest require accretion of chondritic or volatile-bearing material after core formation. The concentrations of Zn, Ag, and Cd modeled for Vesta's core are similar to the concentration range measured in magmatic iron meteorites indicating that these volatile elements were already depleted in Vesta's precursor materials.

INTRODUCTION

The partitioning of siderophile elements between metal and silicate can provide important constraints on conditions prevailing during accretion and core formation in differentiated bodies such as Earth, Mars, and asteroid 4 Vesta. The influence of temperature, pressure, and oxygen fugacity is well known. The nonmetal (e.g., S, C, Si, or O) content of metallic liquids can exert a strong influence on the partitioning of siderophile elements between the core and mantle, and all of these elements are possible candidates for the light element in Earth's core (e.g., Lin et al. 2003; Sanloup et al. 2004; Badro et al. 2007; Mao et al. 2012; Hirose et al. 2013). Although a number of studies have focused on the effect of S and C on partitioning behavior (Chabot et al. 2010; Wood et al. 2014; Liu et al. 2016), relatively little is known about the effect of Si. The effects of Si can be large as has been demonstrated for Mo, and the volatile siderophile elements (VSE) Ge, Sb, As, and P (e.g., Righter et al. 2016, 2017a, 2017b; Vogel et al. 2018). For several important moderately to highly VSE, the effect of Si is unquantified.

Bismuth and Cd are two chalcophile siderophile elements whose partitioning in S- and C-rich systems is

well known, but the behavior in Fe-Si metallic melts is unknown (Li and Audétat 2012, 2015; Kiseeva and Wood 2013). Tin and highly siderophile element (HSE) content of the terrestrial mantle has been used to argue that a Hadean matte segregated from the mantle into the core after the main phase of core formation (O'Neill 1991; Laurenz et al. 2016; Rubie et al. 2016; Ballhaus et al. 2017), yet the arguments were based on few partitioning data for only a moderately chalcophile element (Sn), and none quantifying the effect of a primary core formation event involving Si-rich iron liquid. To evaluate the Hadean matte hypothesis, more data are needed for highly chalcophile elements like the PGE, and Bi and Cd.

The timing of volatile element depletion to Earth's mantle is debated, and some important constraints are provided by the Pd-Ag isotopic system (Schönbächler et al. 2010). There have been hundreds of metal/silicate experiments on Pd published (Righter et al. 2008a; Laurenz et al. [2016] and references therein), but only a handful of Ag experiments (e.g., Jones and Drake 1986; Li and Audétat 2012, 2015; Wheeler et al. 2011). As a result, the effects of important variables on Ag partitioning between metal and silicate are essentially unknown and unquantified. In addition, some volatile elements might retain isotopic evidence for the mechanism of volatile element depletions, such as Sn or Cd (Loss et al. 1990; Wombacher et al. 2003, 2008). Knowledge of the metal/silicate partitioning behavior of these elements can be coupled with the isotopic data to gain a more complete understanding of the budget of these VSE during processes in the early solar system such as accretion, core formation, and differentiation.

Here, we report new experiments designed to quantify the effect of Si on the partitioning of Bi, Cd, Sn, and Ag between metal and silicate melt. The results will be combined with available data (Lupis 1983; Wood et al. [2014] for S and C) to derive a new activity model for these elements in Fe-Ni-Si-S-C liquids. This model will then be combined with previous partitioning data to derive predictive expressions for metal/silicate partitioning of these elements. Finally, we will test the extent to which the Bi, Cd, Sn, and Ag concentrations in the mantles of Earth, Mars, and Vesta were established by core formation or are due to volatility in their precursor materials.

EXPERIMENTAL AND ANALYTICAL APPROACH

Experiments were carried out at 1 GPa and 1600 °C, using a non–end = loaded piston cylinder apparatus; details are similar to those of Righter et al. (2017a) and described in supporting information Section 1. These conditions were chosen to be consistent with previous studies of activity coefficients for trace metals in Fe-Si liquids (e.g., Righter et al. 2017a, 2017b, 2018a, 2018b). The pressure of these experiments is lower than the pressure generally expected during core formation for the Earth. Because there may be pressure effects on the activity coefficients, future studies might also explore higher pressure conditions to assess pressure dependence, but this study was undertaken to establish effects at low pressure. Experimental run products were analyzed for major elements and Bi, Cd, Sn, and Ag using electron microprobe analysis and laser ablation ICP-MS; analytical details are given in supporting information Section 1. Full analyses of the run products are presented in Tables 1 and 2.

RESULTS

Phase Relations and Equilibrium

All experiments consisted of metallic and silicate liquid contained within the MgO capsule (Fig. 1). The metallic melts formed a large spherical ball (or several balls) in the center of each experiment, and typically quenched into dendrites or quench textures comprised of two phases—Fe-rich and Si-rich metals. In almost all experiments, either Bi or Ag was saturated and Bi- and Ag-rich metallic liquids were present sometimes as a free phase and sometimes attached to the edge of a large (hundreds of μm) Fe-Si sphere. There were also smaller blebs of Bi- or Ag-rich metallic liquids within the Fe-Si quenched melts—these are thought to have been dissolved in the Fe-Si melts at run conditions and exsolved upon quench and cooling. Thus, these smaller phases are included in the analysis of the Fe-Si liquids. Silicate liquids also reacted with the MgO capsule and became much more MgO-rich than the starting basalt (as also reported in Righter et al. 2010, 2016, 2017a; Righter 2011). The more MgO-rich silicate melts did not quench to a glass, but instead to several phases including glass and olivine (Fig. 1). In some experiments, MgO crystals also grew from the top of the capsule into the silicate melt.

Equilibrium was achieved or approached in these experiments, as deduced from several lines of evidence. First, the metallic liquids were homogeneous in composition, and did not show any zoning or variation from center to edge of capsule or within the metallic spheres. There are some variations in the trace element concentrations due to quench textures, but overall the trace element contents exhibited no zoning or concentration gradient within the metallic liquids (supporting information Section 1: Fig. S1). Homogeneity in the silicate melts is more difficult to demonstrate due to the presence of coarse quench crystals and quench textures in the MgO-rich silicate melt.

Table 1. Cd and Bi experiments (all experiments at 1 GPa and 1600 °C; values in parentheses are 2σ error).

	CdBi-0	CdBi-2	CdBi-4	CdBi-6	CdBi-10
Silicate (wt%)					
SiO_2	31.6 (1.6)	32.2 (1.6)	35.6 (1.8)	36.5 (1.8)	42.2 (2.1)
TiO_2	3.42 (7)	3.43 (7)	3.15 (6)	2.84 (6)	1.49 (3)
Al_2O_3	11.3 (6)	11.5 (6)	11.1 (6)	10.9 (5)	12.0 (6)
FeO	11.54 (23)	8.91 (18)	0.27 (1)	0.060 (3)	0.010 (5)
MnO	0.150 (3)	0.160 (3)	0.100 (2)	0.060 (2)	0.010 (1)
MgO	26.4 (1.3)	27.1 (1.4)	31.1 (1.6)	34.6 (1.7)	26.0 (1.3)
CaO	11.93 (24)	12.77 (26)	12.82 (26)	11.99 (24)	13.46 (27)
Na_2O	3.0 (2)	3.2 (2)	3.3 (2)	3.0 (1)	3.5 (2)
K_2O	1.81 (4)	1.86 (4)	2.14 (4)	1.85 (4)	2.07 (4)
P_2O_5	0.73 (1)	0.61 (1)	0.030 (1)	0.030 (1)	0.020 (1)
Total	101.87	101.60	99.58	101.74	100.79
Cd (ppm)	1427 (430)	1159 (71)	50.1 (2.9)	26.4 (2.6)	10.6 (1.1)
Bi (ppm)	7.3 (0.6)	8.4 (0.5)	2.6 (0.4)	8.8 (1.2)	1.3 (0.2)
NBO/T	2.62	2.57	2.35	2.52	1.81
Metal (wt%)					
P	0.28 (1)	0.33 (1)	0.68 (1)	0.55 (1)	0.60 (1)
Si	0.034 (1)	0.028 (1)	0.38 (1)	5.82 (12)	18.41 (37)
Bi	0.46 (1)	0.17 (1)	0.34 (1)	0.162 (3)	0.050 (1)
Cd	0.53 (1)	0.62 (1)	0.29 (1)	0.36 (1)	0.133 (3)
Fe	97.41 (1.95)	97.01 (1.94)	97.92 (1.96)	92.25 (1.84)	79.06 (1.58)
Total	98.72	98.16	99.62	99.15	98.25
X_{Si}	0.001	0.001	0.008	0.110	0.313
X_{Fe}	0.99	0.99	0.98	0.88	0.68
ΔIW (Si-SiO_2)	−2.3 (5)	−3.2 (5)	−4.5 (3)	−6.1 (3)	−7.2 (2)
ΔIW (Fe-FeO) activity	−1.67 (3)	−1.90 (3)	−4.94 (8)	−6.04 (35)	−6.64 (42)
ΔIW (Fe-FeO) molar	−2.08 (3)	−2.31 (3)	−5.35 (8)	−6.60 (35)	−7.76 (42)
D(P)	0.38 (2)	0.54 (3)	22.7 (1.8)	18.3 (1.5)	30.0 (2.7)
D(Bi)	630 (70)	202 (25)	1310 (140)	184 (21)	385 (45)
D(Cd)	4.3 (1.3)	5.3 (1.5)	57.9 (15.0)	136 (27)	125 (24)
ln K_d (Fe-P)-1.5 ln γ_{Fe}	−18.2 (7.1)	−19.0 (7.0)	−32.0 (7.2)	−38.6 (7.6)	−40.6 (8.5)
ln K_d (Fe-Bi)-0.5 ln γ_{Fe}	−7.4 (5.1)	−10.3 (5.3)	−18.3 (5.6)	−24.7 (6.1)	−27.2 (7.4)
ln K_d (Fe-Cd)	−1.05 (45)	−0.95 (49)	−2.09 (51)	−2.49 (55)	−3.43 (59)

However, homogeneity is supported by olivine-liquid Fe-Mg K_ds that are consistent with equilibrium and not reflecting a liquid of changing or variable composition. And finally, the diffusion of trace elements at these temperatures is adequate to achieve equilibrium at these experimental length scales and timeframes, as demonstrated previously by Righter et al. (2017a) with time series for the partitioning of As, Sb, Ge, and In. In addition to the time series, the experiments reported here are longer than experiments for which time series have been done for slow diffusing elements such as W^{4+} and P^{5+}, as well as Ga^{3+} and Sn^{4+} (e.g., Righter et al. 1997; Righter and Drake 1999, 2000; Siebert et al. 2011).

Oxygen Fugacity

As mentioned above, Si metal was added to experiments to promote more reduced conditions—Si alloys with Fe at high temperatures, and an increase in Si content will cause a decrease in fO_2. Oxygen fugacity was calculated relative to the iron-wüstite (IW) oxygen buffer using two different equilibria. First, the equilibrium $Si + O_2 = SiO_2$ was used along with the thermodynamic data from Robie et al. (1978), γ Si calculated using Righter et al. (2017a) model, and assuming γ $SiO_2 = 1$. Because the amount of Si in the metal is high (and FeO is very low) at low fO_2, this equilibrium is more robust at lower fO_2. Oxygen fugacity can be estimated using a second equilibrium, $Fe + ½ O_2 = FeO$, using the expression $\Delta IW = -2 \log[X_{Fe}/X_{FeO}]$. Because the amount of Fe in the metal is high (and FeO in the silicate melt is high) at higher fO_2, this equilibrium is more robust at higher fO_2s. The ΔIW values ranged from ~ −2.08 (for Si-free runs) to −5.25 to −7.91 (for Si-bearing runs) (Tables 1 and 2). If the activities of Fe and FeO are considered, the equation becomes $\Delta IW = -2 \log[a_{Fe}/a_{FeO}]$. In this case, a_{Fe} can be calculated using the epsilon parameter activity

Table 2. Ag and Sn experiments (all experiments at 1 GPa and 1600 °C; values in parentheses are 2σ error).

	SnAg-0	SnAg-2	SnAg-4	SnAg-6	SnAg-10
Silicate (wt%)					
SiO_2	32.1 (1.6)	33.3 (1.7)	41.8 (2.1)	43.0 (2.2)	44.2 (2.2)
TiO_2	3.58 (7)	3.97 (8)	3.56 (7)	3.32 (7)	1.81 (4)
Al_2O_3	11.8 (6)	13.4 (7)	12.4 (6)	12.4 (6)	11.6 (6)
FeO	10.51 (21)	4.41 (9)	0.110 (2)	0.030 (1)	0.010 (1)
MnO	0.140 (3)	0.170 (3)	0.130 (3)	0.080 (2)	0.020 (1)
MgO	25.8 (1.3)	26.5 (1.3)	24.0 (1.2)	22.4 (1.2)	25.5 (1.1)
CaO	12.53 (25)	14.29 (29)	13.81 (28)	13.77 (28)	12.94 (26)
Na_2O	3.4 (2)	3.9 (2)	3.7 (2)	3.7 (2)	3.5 (2)
K_2O	2.03 (4)	2.20 (4)	2.14 (4)	2.15 (4)	2.02 (4)
P_2O_5	0.71 (1)	0.180 (4)	0.050 (1)	0.070 (1)	0.040 (1)
Total	102.60	102.25	101.69	100.97	101.54
Sn (ppm)	343 (48)	83 (13)	8.0 (1.4)	4.20 (83)	2.80 (62)
Ag (ppm)	132 (20)	61.4 (10.1)	13.9 (2.6)	9.0 (1.9)	9.2 (2.3)
NBO/T	2.52	2.27	1.71	1.59	1.72
Metal (wt%)					
P	0.240 (5)	0.65 (1)	0.67 (1)	0.79 (2)	0.67 (1)
Si	0.0020 (1)	0.010 (1)	3.05 (6)	8.55 (17)	17.09 (34)
Sn	4.22 (8)	3.42 (7)	2.79 (6)	2.37 (5)	1.29 (3)
Ag	0.67 (1)	0.59 (1)	0.35 (1)	0.180 (4)	0.090 (2)
Fe	95.23 (1.90)	96.31 (1.93)	92.78 (1.86)	89.03 (1.78)	81.81 (1.64)
Total	100.36	100.98	99.64	100.92	100.95
X_{Si}	0.0004	0.0009	0.061	0.160	0.297
X_{Fe}	0.97	0.97	0.91	0.82	0.69
ΔIW (Si-SiO_2)	−3.1 (5)	−3.4 (5)	−5.7 (3)	−6.3 (3)	−7.2 (2)
ΔIW (Fe-FeO) activity	−1.74 (2)	−2.50 (2)	−5.55 (6)	−6.37 (20)	−6.81 (50)
ΔIW (Fe-FeO) molar	−2.15 (2)	−2.91 (2)	−6.06 (6)	−7.08 (20)	−7.91 (50)
D(P)	0.34 (5)	3.6 (3)	13.4 (1.1)	11.3 (9)	16.8 (1.3)
D(Sn)	123 (10)	412 (39)	3490 (420)	5640 (680)	4610 (550)
D(Ag)	50.8 (6.1)	96.1 (11.5)	252 (20)	200 (16)	97.8 (11.7)
ln K_d (Fe-P)-1.5 ln γ_{Fe}	−18.9 (7.0)	−19.9 (7.4)	−36.0 (7.5)	−40.5 (7.8)	−42.3 (8.2)
ln K_d (Fe-Sn)-ln γ_{Fe}	0.9 (2.0)	−0.4 (1.8)	−6.1 (2.2)	−7.8 (2.4)	−9.5 (2.7)
ln K_d (Fe-Ag)	0.53 (0.50)	0.93 (51)	−0.80 (61)	−1.84 (62)	−2.69 (72)

model for metallic liquids presented by Righter et al. (2017a), and a_{FeO} can be calculated in silicate melt using the results of Holzheid et al. (1997). ΔIW values calculated using activities instead of mole fractions are slightly higher, ranging from IW−1.67 to −6.81 (Tables 1 and 2). Because most studies utilize X_{Fe}/X_{FeO} to calculate ΔIW, we include those values in the tables and figures, but it is important to note the difference in these approaches given the nonideality in the Fe-Si-C system. The fO_2s calculated with activities are used in later calculations in the Mars section: the Fe-FeO equilibrium is used for experiments with 0, 2, and 4 wt% Si added, because FeO in the silicate is high and Si in the metal is low. Whereas the Si-SiO_2 equilibrium is used for experiments with 6 and 10 wt% Si added, where FeO in the silicate is lower (and has higher uncertainty), but Si in the metal is higher. The range of ΔIW values for these experiments falls in the range typically considered during Earth's core formation.

Metal/Silicate Partition Coefficients

A standard approach for partitioning uses the distribution coefficient which is simply the weight ratio of the element in the metal and the silicate melt, or *D*(i) metal/silicate = wt fraction i in metal/wt fraction i in silicate melt. The influence of oxygen fugacity on partition coefficients is usually assessed by plotting *D* (met/sil) versus log fO_2, where D increases with decreasing fO_2 according to the valence of the element in question. For example, a 3+ element will have a slope of 0.75, 2+ a slope of 0.5, and 1+ a slope of 0.25. This approach cannot be used in experiments where the metallic liquid contains Si, because the activity coefficient for the trace siderophile element of interest is strongly dependent on the Si content (e.g., Righter et al. 2017a, 2018b; Tuff et al. 2011; Vogel et al. 2018). Silicon causes a decrease in metal/silicate D which strongly modifies the classic trend of log *D* versus

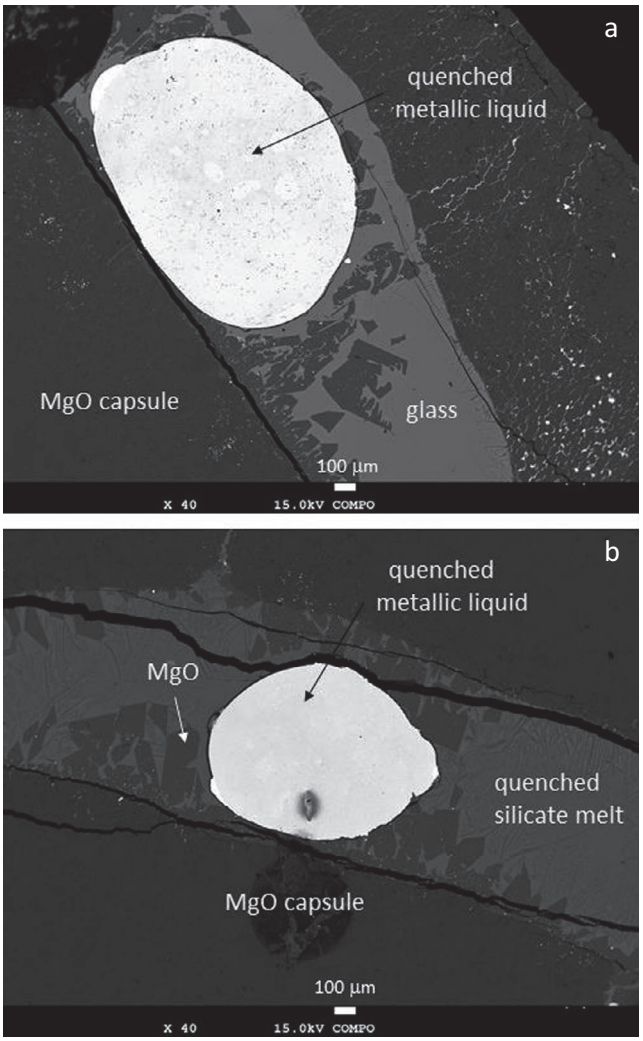

Fig. 1. a) Backscattered electron image of experiment Cd-Bi-10 equilibrated at 1 GPa, 1600 °C, with ~17 wt% Si in the metal. Bright rounded phase is Fe-Si-P-Bi-Cd alloy and light gray phase is silicate melt; some MgO capsule material (darkest phase) is also present in the silicate melt. b) Backscattered electron image of experiment Sn-Ag-4.

log fO_2. Instead of examining this partition coefficient D, we use the exchange coefficient with Fe to determine the activity coefficient of these five metals in Fe-Si liquids, as shown next.

Determination of Epsilon Interaction Parameters

Measured Bi, Cd, Sn, and Ag, and other siderophile elements were used to calculate metal (met)—silicate (sil) exchange K_d according to this equation (where n = valence of element M in silicate melt):

$$MOn/2_{sil} + (n/2)Fe_{met} + (n/2)FeO_{sil} \quad (1)$$

Expanding Equation 1 and following a similar approach to Righter et al. (2017a),

$$\ln K = \ln \frac{\left[a_M^{metal}\right]\left[a_{FeO}^{silicate}\right]^{n/2}}{\left[a_{MO(n/2)}^{silicate}\right]\left[a_{Fe}^{metal}\right]^{n/2}} = \ln \frac{\left[X_M^{metal}\right]\left[X_{FeO}^{silicate}\right]^{n/2}}{\left[X_{MO(n/2)}^{silicate}\right]\left[X_{Fe}^{metal}\right]^{n/2}} + \ln \frac{\left[\gamma_M^{metal}\right]\left[\gamma_{FeO}^{silicate}\right]^{n/2}}{\left[\gamma_{MO(n/2)}^{silicate}\right]\left[\gamma_{Fe}^{metal}\right]^{n/2}} \quad (2)$$

We set $K_d \frac{\left[X_M^{metal}\right]\left[X_{FeO}^{silicate}\right]^{n/2}}{\left[X_{MO(n/2)}^{silicate}\right]\left[X_{Fe}^{metal}\right]^{n/2}}$ and assume the ratio of oxide activity coefficients in the silicate, $\frac{\left[\gamma_{FeO}^{silicate}\right]^{n/2}}{\left[\gamma_{MO(n/2)}^{silicate}\right]}$, is fixed, since the silicate melt compositions are nearly constant in this study. On the other hand, the metal composition varies significantly in Si content and the ratio of activity coefficients in the metal, $\frac{\left[\gamma_M^{metal}\right]}{\left[\gamma_{Fe}^{metal}\right]^{n/2}}$, is dependent upon variation in metal composition. The above equations can be rearranged to yield:

$\ln K_d = \text{constant} + n/2 \ln \gamma_{Fe}^{metal} - \ln \gamma_M^{metal}$. When combined with $\ln \gamma_M^{metal} = \ln \gamma_{Fe}^{metal} + \ln \gamma_M^0 - \varepsilon_M^{Si} \ln (1-X_{Si})$ yields $\ln K_d - (n/2\text{–}1) \ln \gamma_{Fe}^{metal} = \text{const} - \ln \gamma_M^0 + \varepsilon_M^{Si} \ln (1-X_{Si})$. Here ε_M^{Si} is an interaction parameter (e.g., Lupis 1983) that can be used to isolate the effect of a solute such as Si (in Fe metallic liquid) on the activity of a trace element such as Bi, Cd, Sn, and Ag (or see Righter et al. [2017a] for As, Sb, In, and Ge). The slope of $\ln K_d$ versus $\ln(1-X_{Si})$ gives ε_M^{Si} directly for each element at 1600 °C. This approach ignores interactions between trace elements but these are likely to be small compared to the effect of Si (a major element) on the trace element of interest.

Phosphorus serves as an example of how this approach works. The Si-free samples equilibrated at fO_2 values of IW-2, and where P is largely stable in the silicate melt as P_2O_5. The experiments with most Si-rich metals equilibrated at fO_2 values as low as IW-6, where the Fe and P are nearly entirely reduced to the metal, and P_2O_5 and FeO contents of the silicate melt are very low (Fig. 2; P not shown, only FeO). Measured P and Fe in metal and silicate were used to calculate metal (met)—silicate (sil) exchange K_d according to: $P_2O_5^{sil} + 5Fe^{met} = 2P^{met} + 5FeO^{sil}$. From this equilibrium, activity coefficients are derived for P in Fe-Si liquids (see Righter et al. 2017a). The valence of P in silicate melts is assumed to be 5+ for these calculations in agreement with previous studies (e.g., Righter et al. 2017a, 2017b; Siebert et al. 2011).

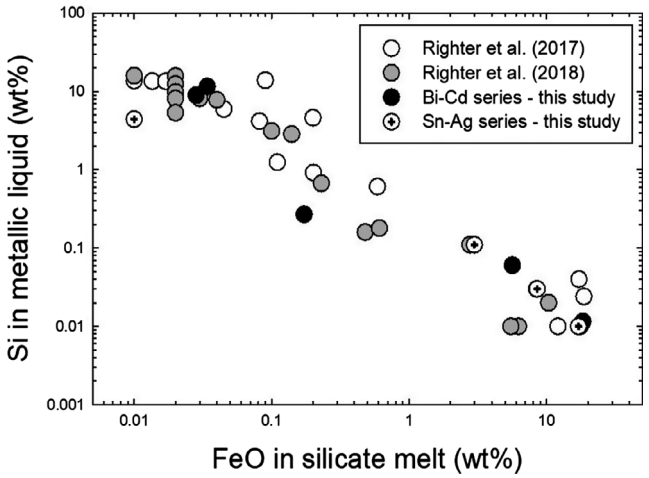

Fig. 2. Negative correlation between Si content of the Fe metal and FeO content of the silicate melt. Our new results for the experiments with Fe-Sn-Ag-Si-P and Fe-Bi-Cd-Si-P show similar behavior to previous experimental series with variable Si content of metal from Righter et al. (2017a, 2017b, 2018a, 2018b).

We have determined ε_M^{Si} for Bi, Cd, Sn, and Ag (Fig. 3). All four elements have positive epsilon parameters, 42.5 (18.7), 5.6 (1.7), 27.9 (8.9), and 10.0 (2.0), respectively, at 1 GPa and 1600 °C, indicating that dissolved Si causes a decrease in their partition coefficients (Fig. 3). For these elements, the assumed valence (for Equation 1) of Bi is 3+ (e.g., Righter et al. 2018a, 2018b), Sn = 4+ (e.g., Capobianco et al. 1999; this study), and Cd and Ag = 2+ (e.g., Wheeler et al. 2011; Wang et al. 2016). Although evidence for Sn^{2+} is presented in the literature, regression of activity corrected D(Sn) values results in a ln fO_2 term near −1 that suggests Sn^{4+} is stable across the fO_2 range of the studies included (Table S4 in supporting information). However, for completeness, we have also calculated ε_{Sn}^{Si} assuming Sn^{2+}, and the resulting value is 12.6(3.2). Because the basalt contains significant P, we also have derived interaction parameters for P. As we have shown in previous experiments involving Pt, Pd, and Au, phosphorus exhibits high and positive epsilon values of 56.8(15.5) (comparable to values of 66 and 69 derived in previous studies of Righter et al. 2018a, 2018b).

Calculation of Activity Coefficients in Fe-Ni-Si-C-S Liquids

The activity model of Ma (2001) and Wade and Wood (2005) was coded in MATLAB, and expanded to include the newly acquired epsilon interaction parameters in Fe-Si liquids for Bi, Cd, Sn, and Ag (from this work) and in Fe-S liquids for Cd, Bi, Sn, and In (using experiments from Righter et al. 2017b). This model includes recent data of As, Sb, Ge, and In (Righter et al. 2017a), Au, Pd, Pt, P, Ga, Cu, Zn, and Pb (Righter et al. 2018b), as well as previously determined epsilon parameters for Fe-S and Fe-C liquids for these elements (Steelmaking Data Sourcebook 1988; Wood et al. 2014). We added Bi and used the ln γ_0 value of 6.87 (Chang et al. 1998). Our new epsilon values for Bi, Cd, Ag, and Sn demonstrate that all four elements will become less siderophile with the addition of Si. Furthermore, the effect of Si is much stronger and opposite than S (supporting information Section 2: Table S1). However, because the epsilon (Fe-Si) values for each element are positive and of greater magnitude than the epsilon (Fe-S) values, the chalcophile behavior of these five elements will be completely erased when Si is dissolved in Fe metallic liquid (Fig. 4).

This updated model allows us to calculate the activity of Bi, Cd, Sn, and Ag (as well as 30 other elements; Table S2 in supporting information) in Fe-Ni-Si-S-C metallic liquids. As an example of how large the effect of Si can be, these epsilon values correspond to activity coefficients (γ) for Cd, for example of ~1 when $X_{Si} = 0$, up to $\gamma \sim 5$ when $X_{Si} = 0.2$ (Fig. 5). Similarly, γ increases by a factor of nearly 10 across this range for Ag, and changes dramatically for Sn due to the large interaction parameter for Sn (27.9) we measured in this study. It is clear that Si has an enormous effect on the activity coefficient and metal-silicate partitioning behavior of P, Bi, and Sn, and significant effect on Ag and Cd. As discussed by Righter et al. (2017a), this may be related to a lower tendency of these elements to form silicides; Bi, Sn, Ga, Sb, and In, for example, do not form silicides in the M-Si phase diagrams, and all have positive and high values.

VSE CONCENTRATIONS IN SILICATE MANTLES

Depletions of Bi, Cd, Ag, Sn in Earth, Mars, Vesta

Processes Responsible for Depletions

Righter et al. (2018a, 2018b) present a detailed discussion of the various processes that may contribute to the depletion of a volatile siderophile element in the mantle of a differentiated body. These include precursor volatile element depletions (e.g., Lodders 2003; Norris and Wood 2017), core formation (e.g., Righter and Drake 2000; Righter et al. 2017a, 2017b), sulfide segregation from a magma ocean (e.g., O'Neill 1991; Rubie et al. 2016; Righter et al. 2018a, 2018b), sulfide retention during mantle melting (e.g., Righter et al. 2008a, 2008b, 2015), and magmatic degassing (from a magma ocean or from later localized magmas; Paniello et al. 2012; McCubbin et al. 2015; Barnes et al. 2016).

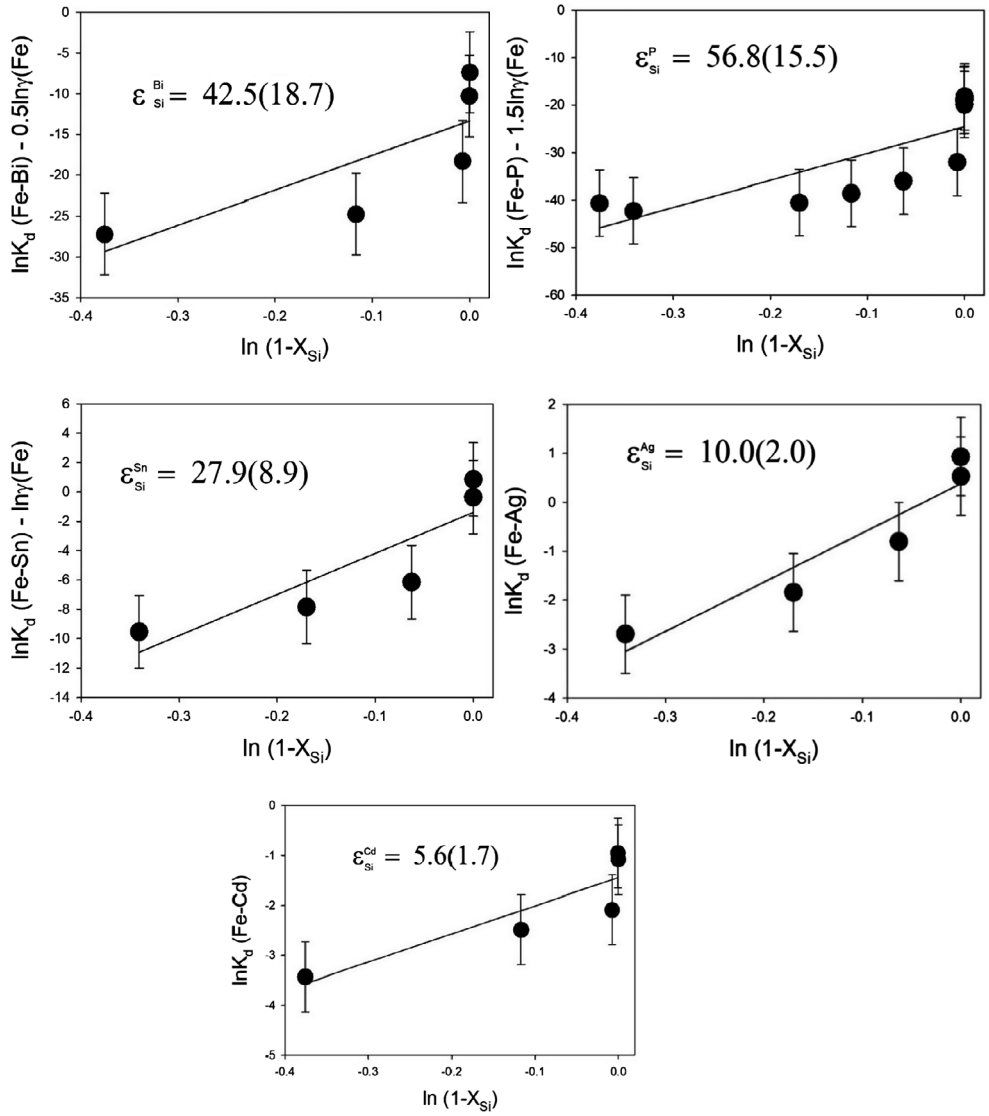

Fig. 3. ln K_d(Fe-M) versus ln(1 − X_{Si}) for Bi, P, Sn, Ag, and Cd at 1600 °C. Solid lines are a linear fit to the data, the slope of each line is the ε_M^{Si}, and associated error is in parentheses.

Most of the VSE—and specifically those studied here P, Bi, Cd, Ag, and Sn—are incompatible during melting of the mantle. Therefore, if a mantle VSE content has been set by precursor volatile element depletion and later core formation, and is then melted, the melts generated will have higher VSE content than the mantle due to the incompatibility. As a result, if a VSE is plotted against a refractory lithophile element (RLE) of similar incompatibility, the two elements will define a 1:1 linear trend (e.g., Wanke and Dreibus 1986). Such examples can be seen in many siderophile—RLE pairs such as P-Nd, Mo-Pr, or W-U (e.g., Wanke and Dreibus 1986). The linear trend, coupled with an estimate of the RLE content of a mantle, can be used to estimate the VSE content of the mantle before melting.

Correlations between Bi-Yb, Cd-Yb, In-Yb, Sn-Sm (VSE–RLE pairs) define VSE depletions in Earth, Mars, and Vesta as we will see in the discussions below. The role of all these processes—precursor volatility, core formation, Hadean sulfide matte, magmatic sulfide segregation, and magmatic volatility—must be assessed so their effect on VSE concentrations in Martian, lunar, or terrestrial basalt can be interpreted. Sulfide fractionation is known to affect the most chalcophile elements which are Bi, Cu, and Ni, whereas Cd, Pb, and Co are intermediate and As, Mo, Sn, and Sb relatively low in chalcophility (e.g., Li and Audétat 2012; Kiseeva and Wood 2013). Degassing is known to affect many elements, including many of the VSE. It is well known from studies of

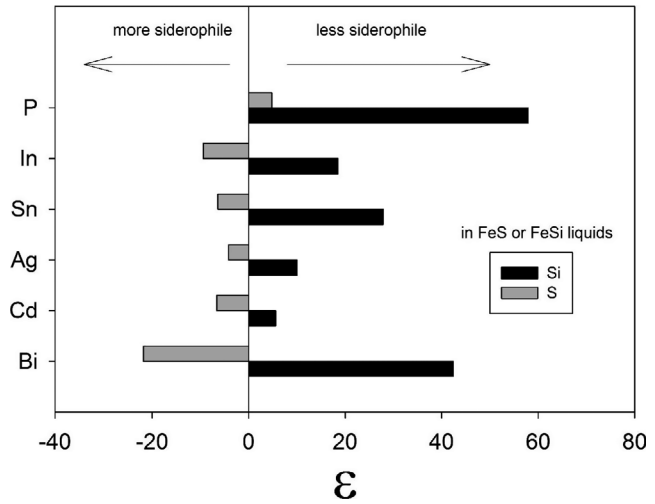

Fig. 4. Comparison of epsilon values for Bi, Cd, Sn, Ag, and P in Si-bearing Fe metallic liquid to those determined in previous studies for S-bearing metallic liquids (Wood et al. 2014).

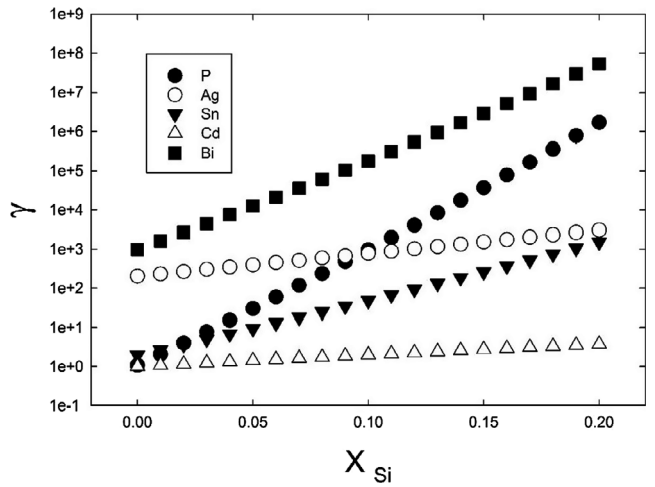

Fig. 5. ln $\gamma(M)$ for Bi, Cd, Sn, Ag, and P versus mole fraction of Si in the metallic Fe liquid, calculated at 1600 °C, showing the strong effect of dissolved Si on the activities of these metals. ln $\gamma(M)$ values are calculated using epsilon parameters derived here, tabulated in Wade and Wood (2005) and Wood et al. (2014), and used in the Wade and Wood (2005) MetalAct model, using modified version of Ma (2001).

trace metals in volcanic gases that many VSE can be concentrated in the gas phase (Rubin 1997; Norman et al. 2004), with Bi and Cd being strongly concentrated (emanation coefficients of 0.31 and 0.26, respectively), and Sn and In being less strongly but nonetheless high (emanation coefficients of 0.0012 and 0.0018, respectively). Degassing might account for concentration drops of 2× to 3× in Cd and Bi contents (Righter et al. 2018a, 2018b). Diffusion studies of As, Sb, Cd, Bi, and Pb have been carried out by MacKenzie and Canil (2008) and Johnson and Canil (2011), and all five of these elements have high diffusion coefficients that would allow mobility under magmatic conditions. If a solid understanding exists of these processes, then mantle concentrations of VSE in Mars and Vesta can be estimated using knowledge of the geochemical behavior.

Depletion of Ag, Sn, Bi, and Cd in Mantles of Differentiated Bodies

Depletions of Sn, Bi, and Cd in the Earth, Moon, and Mars were defined in Righter et al. (2018a, 2018b) and will not be described in detail again; the reader is referred to that work for a detailed description of data and approaches used. Depletions of Sn, Bi, and Cd in the mantle of Vesta are newly derived here, using the data of Paul and Lipschutz (1990), Cleverly et al. (1986), Kiesl et al. (1978), Morgan et al. (1978), and De Laeter et al. (1974) (see supporting information Section 3). Silver depletions for multiple bodies have not been considered in recent studies, although separate studies on individual bodies have been completed (e.g., Wolf et al. [1979] for Moon, Treiman et al. [1986] for Mars, or Paul and Lipschutz [1990]). We examine and compile literature sources of Ag data (aided by the compilation of Mittlefehldt 2015) and derive new estimates for Moon, Mars, and Vesta (Fig. 6; supporting information Section 3). A summary of the Sn, Bi, and Cd depletions and the corresponding mantle concentration estimates for Earth, Mars, and Vesta appear in Table S3 in supporting information.

Application to Core Formation and Metal-Silicate Partitioning

Calculating Mantle Concentrations of VSE

Mantle concentrations of siderophile elements after core formation can be calculated according to (from Righter et al. 2016):

$$C^i_{LS} = \frac{C^i_{bulk}}{x\left[p + (1-p)D^i_{SS/LS}\right] + (1-x)\left[D^i_{LM/LS}\right]} \quad (3)$$

where x is the fraction of silicate, p is the fraction of molten silicate, C^i_{bulk} is the bulk concentration of siderophile element, C^i_{LS} is the concentration of siderophile element in the liquid silicate, $D^i_{LM/LS}$ is the partition coefficient between solid silicate and liquid silicate (<0.1 for all elements here), and $D^i_{LM/LS}$ (=$D(i)$ from Equation 4 below) is the partition coefficient between liquid metal and liquid silicate). For Earth calculations, x = 0.68 and p = 0.6, for Mars x = 0.78 and p = 0.6, and for Vesta x = 0.82 and p = 1.0 (from Righter and Drake 1997;

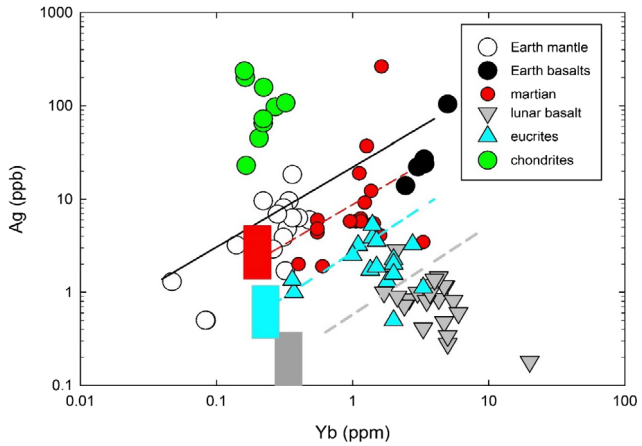

Fig. 6. Correlation between Ag and Yb in a variety of samples including chondrites, terrestrial mantle (from Morgan et al. 1980; Wang and Becker 2017), terrestrial basalt (Hertogen et al. 1980), lunar basalt (Wolf et al. 1979), Martian shergottites (Laul et al. 1972; Smith et al. 1984; Wang and Becker 2017), and Vesta (Paul and Lipschutz 1990). Rectangular vertical boxes represent the estimates for the mantle concentration of Ag for Mars (red), Moon (gray), and Vesta (light blue). Primitive terrestrial upper mantle value is from Palme and O'Neill (2014). (Color figure can be viewed at wileyonlinelibrary.com.)

Righter 2011; Yang et al. 2015, respectively). The bulk composition and partition coefficients are specified in more detail.

Bulk Compositions and Volatile Depletions

The bulk compositions of Earth, Mars, and Vesta have been estimated in previous studies—we assume CI compositions from Palme and O'Neill (2014) for Earth, the Lodders and Fegley oxygen isotope model for Mars (Lodders and Fegley 1997), and the L-CV mixture for Vesta (Righter et al. 1997). Each of these bulk compositions must then be corrected for volatility since all three bodies exhibit volatile lithophile element depletions relative to chondrites; the Bi, Cd, Sn, and Ag concentrations must all be adjusted for volatility as follows. For Earth, volatile elements are corrected as described and tabulated by Palme and O'Neill (2014). For Mars, the volatile lithophile trend in the Martian mantle is used to correct the bulk composition of Lodders and Fegley (1997) for volatility (see Righter et al. 2018a, 2018b). And finally, the Vesta bulk composition of 0.7L-0.3CV chondrite mixture (Boesenberg and Delaney 1997; Righter and Drake 1997) is corrected for volatility using K/La, Na/La, Rb/La, and Cs/La ratios from eucrite compositions tabulated by Kitts and Lodders (1998). The bulk compositions (before and after volatility corrections) are summarized in Table S3 in supporting information and shown graphically in Fig. 7. In general, Mars volatility corrections are the smallest, followed by Earth corrections which are modest, and Vesta corrections which are the largest as expected from its severe lithophile volatile depletions such as the alkalis.

Regressions

All partitioning data have been combined and regression performed to create predictive expressions for $D(i)$ metal/silicate according to this equation which has been derived elsewhere (Righter et al. 2017a; supporting information Section 4).

$$\ln D(i) = a \ln fO_2 + b/T + cP/T + \ln \gamma_i + g[\mathrm{nbo}/t] + h \quad (4)$$

Our new data for Sn and Cd are combined with the data sets used in the regression analysis presented by Righter et al. (2018a, 2018b). In addition, the recent study of Ballhaus et al. (2017) extends to higher pressure and temperature and understanding of D(Sn). Data for Bi and Ag are sparse but can be combined to derive expressions to predict metal-silicate partition coefficients. Bi has been studied in S-bearing systems by Li and Audétat (2012), and Si-bearing systems in this study. In addition, effects of higher pressure and temperature were reported by Righter et al. (2019) to conditions of 2200 °C and 20 GPa. Silver partitioning data include studies of Jones and Drake (1986), Li and Audétat (2012), Kiseeva and Wood (2013), and Wood et al. (2014) in S-bearing systems, and the higher temperatures and pressure of Wheeler et al. (2011) and Righter et al. (2019). Our new results extend the metal compositional range to include Si-bearing metallic liquids. All of the regression results are summarized in Table S4 in supporting information. Table S4 also includes regression results for Zn and In, which were studied by Righter et al. (2018a, 2018b), and included in this modeling because they are also both volatile.

The a terms ($\ln fO_2$) are consistent with Sn^{2+}, Ag^{2+}, and Cd^{2+}, as expected and demonstrated previously (Righter et al. 2018a, 2018b); our term for Bi is lower than expected for Bi^{3+}, suggesting that there may be some Bi^{2+} at higher PT conditions, but this should be the focus of a future investigation. Temperature causes an overall decrease in $D(i)$ metal/silicate (Righter et al. 2018a, 2018b). Pressure terms are mostly positive (some are slightly negative), and thus might be expected to cause increase in $D(i)$ metal/silicate, but pressure is coupled with the absolute $\ln fO_2$ such that increase in pressure is associated with increase in fO_2 which causes (especially for high valence elements) a decrease in $D(i)$. The activity coefficient

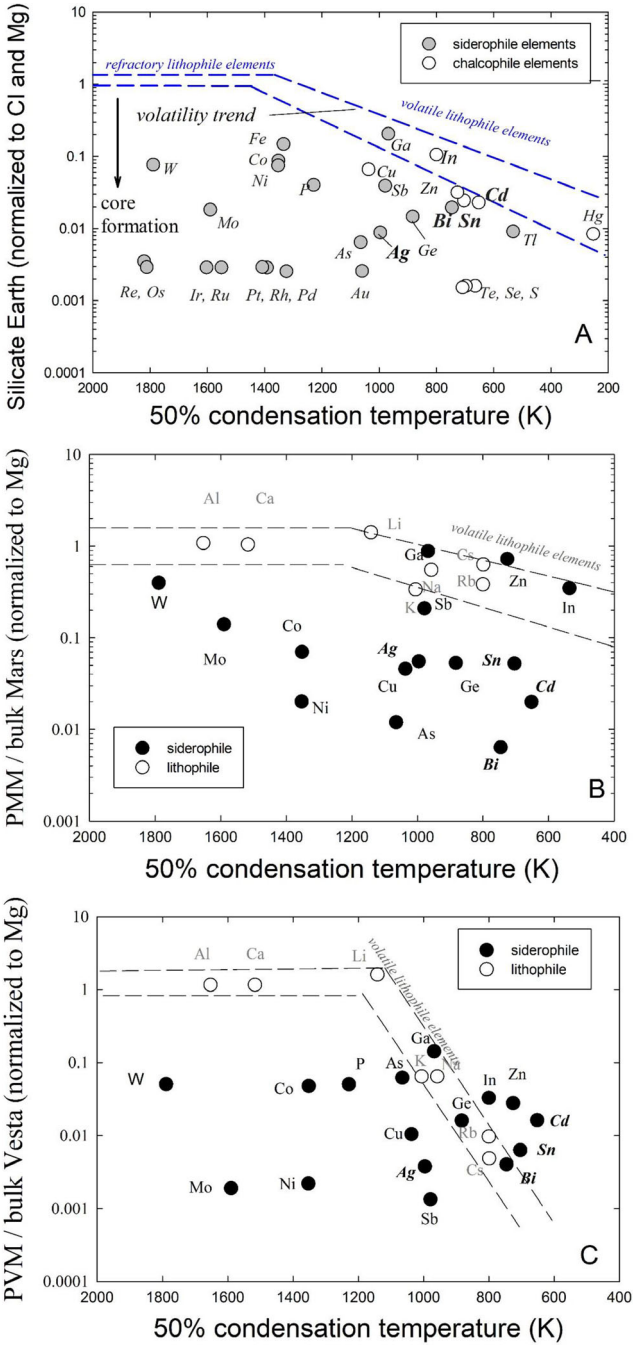

Fig. 7. Concentrations of siderophile elements in the terrestrial primitive upper mantle, relative to CI chondrites and normalized to Mg, plotted against 50% condensation temperature for the metal (after Palme and O'Neill 2014). Depletions of volatile siderophile elements are due in part to volatility, as shown by the region between dashed lines. Bi, Cd, Sn, Ag, and P plot below the volatility trend indicating that a further depletion is likely due to core formation. Condensation temperatures for elements are commonly tabulated in 50% values (taken from Lodders 2003), which indicate the temperature at which the element falls to 50% of its initial value in the gas (e.g., Wasson 1985); the abundances of the volatile elements are thought to be a reflection of condensation processes in the early solar nebula. Volatility corrections for Bi, Cd, Sn, and Ag are 10, 10, 10, and 3, respectively, based on Fig. 6a (see text for more details). Mars volatile element depletions are based on Lodders and Fegley (1997) bulk Mars composition and mantle concentrations of Taylor (2013) and Righter et al. (2015, 2018a, 2018b). Volatility corrections for Bi, Cd, Sn, and Ag in bulk Mars are 3, 3, 3, and 1.5, respectively, based on Fig. 6b (see text for more details). Vesta volatile element depletions are based on the 70%L–30%CV chondrite mixture for the bulk Vesta (Righter and Drake 1997), with mantle concentrations from Righter et al. (2011), Righter et al. (2018a, 2018b) and Steenstra et al. (2016). Volatility corrections for Bi, Cd, Sn, and Ag in bulk Vesta are 500, 500, 500, and 10, respectively, based on Fig. 6c (see text for more details). All volatility corrections, including those for P, Zn, and In, are summarized in Table S3. (Color figure can be viewed at wileyonlinelibrary.com.)

of each element, $\ln \gamma_i$, is calculated using the ε interaction parameter model of Righter et al. (2017a) with new ε interaction parameters and γ_0 from this study and those of Righter et al. (2017a, 2018a, 2018b). Carbon and silicon dissolved in Fe metallic liquid both cause a decrease in D for all four of these elements, whereas S causes all to increase, consistent with the chalcophile behavior traditionally assumed for these elements.

Earth

Earth likely accreted from material that started reducing and became more oxidized over time (e.g., Wood et al. 2006; Righter et al. 2017a). The early reduced nature would have favored Si dissolution into the core, as would later conditions at higher pressure. As the Earth accreted, then, the core-forming metallic liquid changed composition over time, and when coupled with changes in fO_2, temperature and pressure, the resulting mantle concentrations of these elements changed as well (Fig. 8). Following the approach of Righter et al. (2017a), the S, C, and Si content of the core Fe-Ni metal can be calculated as accretion proceeds with increasing pressure and temperature and two different fO_2 scenarios: fO_2 changing from reduced to oxidized (IW-4 to IW-2) and fO_2 constant. The composition of the accreting material does not change in this model—only the partitioning of Fe between metal and silicate in response to fO_2 changes. The model core composition (Fe, Ni, S, C, and Si components) can then be used to calculate the activity coefficient and thus D(metal/silicate) for the VSE using Equation 3. Coupling the calculated values of D metal/silicate with Equation 4, and assuming metal-silicate equilibration occurs

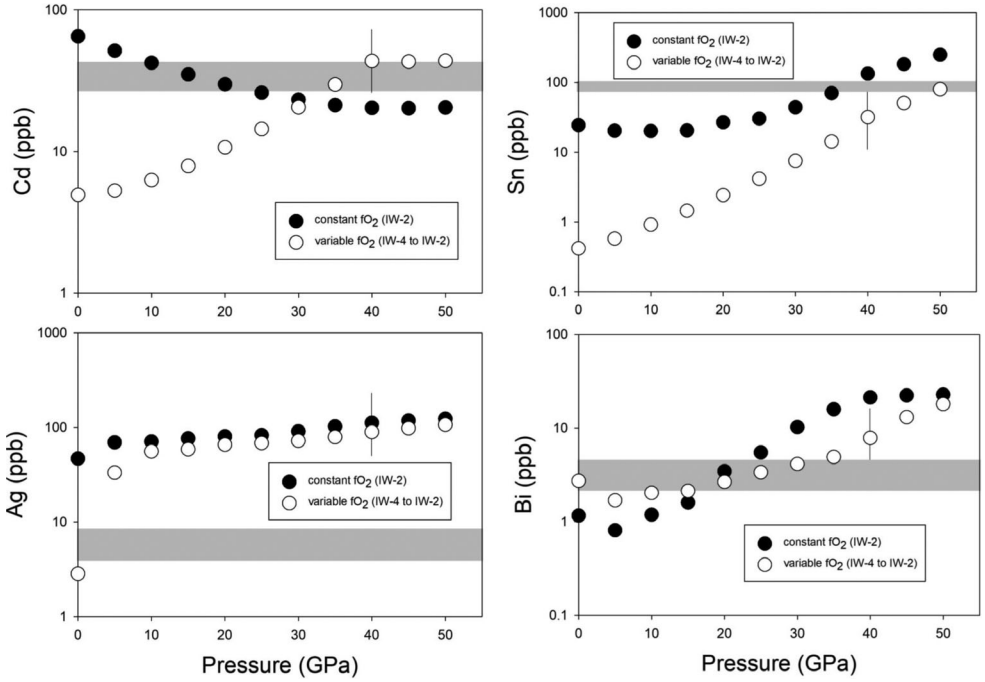

Fig. 8. Evolution of Earth's mantle volatile siderophile elements as accretion proceeds for two different scenarios: accretion with fO_2 nearly constant (filled circles), and fO_2 increasing (open circles). PT curve for calculations is along peridotite liquidus of Andrault et al. (2011). Horizontal bands represent terrestrial primitive upper mantle values (and associated uncertainty) for each element, from Table S3. Error bars on calculated values are representative error for specific elements (2σ) from uncertainty in regressions presented in Table S4.

rapidly during metal droplet "rainfall" through the mantle (Kendall and Melosh 2016) allows calculation of the mantle concentrations of Bi, Cd, Ag, Sn, and P. In a scenario where fO_2 is constant (at IW-2) during accretion, concentration of Ag and Bi becomes overabundant in the mantle at the high PT conditions expected during core formation, while Cd and Sn come closer to primitive mantle values. Consideration of variable fO_2 during accretion (from IW-4 to IW-2) results in similar resulting mantle concentrations near 50 GPa and 3800 K (Fig. 8). The end result of this fO_2 pathway is shown in Fig. 9a, where the concentrations of all elements in the mantle, calculated for metal-silicate equilibrium between the metallic core and peridotite mantle, are compared to concentrations measured in peridotite (the final core composition in the variable fO_2 model is 9% Ni, 10.2% Si, 2% S, and 1.1% C, consistent with studies arguing an Si-rich terrestrial core; e.g., Hirose et al. 2013). The match is good for five elements considered here—Cd, Sn, and P, as well as Zn and In, as well as many other elements such as argued previously by Righter et al. (2017a, 2017b, 2018a, 2018b) (supporting information Section 5, for Ni, Co, Mo, and W). For Earth, these elements then can be explained by a combination of volatile-depleted precursor material, plus core formation.

However, two elements—Bi and Ag—are significantly higher than primitive upper mantle (PUM) estimates, and require a removal mechanism to attain the lower PUM levels. Segregation of a late sulfide matte from the terrestrial mantle has been argued based on several HSEs such as Pd and Au which become overabundant in the mantle during core formation (e.g., Rubie et al. 2016; Righter et al. 2018a, 2018b). Because Bi and Ag are also chalcophile elements, their overabundance in the magma ocean after core formation could thus also be solved by segregation of a sulfide matte. This finding now extends the number of elements requiring segregation of a late sulfide matte and provides new strong evidence for this early stage of terrestrial mantle evolution.

Mars

Previous studies of the Martian mantle have suggested that Mars experienced a mid-mantle (~14 GPa) differentiation event that affected slightly and moderately siderophile elements, as well as lithophile isotopic systems such as Lu-Hf and Sm-Nd

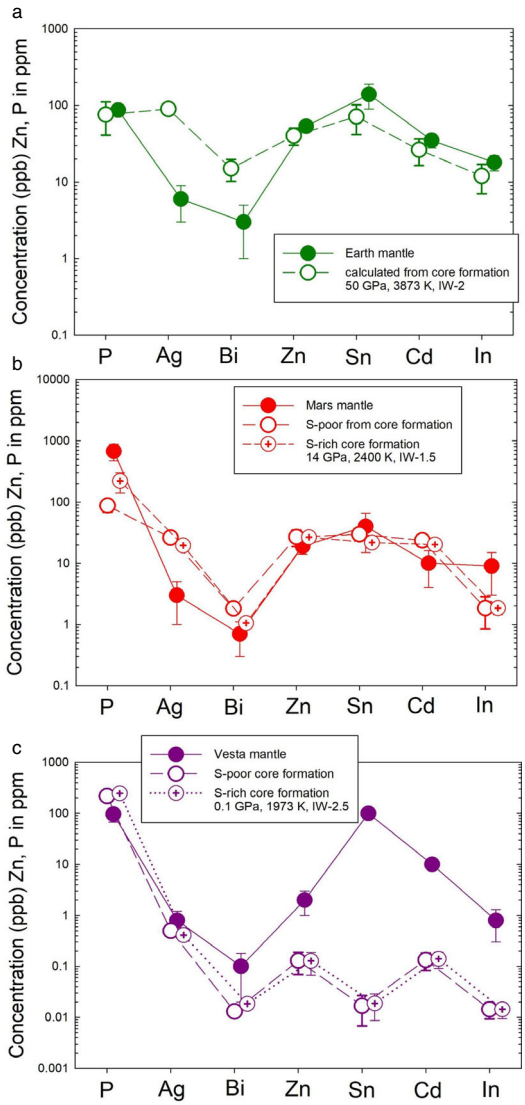

Fig. 9. Comparison of mantle concentration estimates of Bi, Cd, Sn, Ag, P, Zn, and In for Earth (a), Mars (b), and Vesta (c) (open circles) to the calculated mantle values after core-mantle equilibration at the indicated conditions. Five out of the seven elements for Earth's mantle can be explained by core formation and volatile-element depleted precursors, except for Bi and Ag which require a removal mechanism such as late sulfide segregation. Most elements in the mantle of Mars can be explained by core formation and volatile element depleted precursors. For Vesta, only Ag and P can be explained by core formation and volatile element depleted precursors, but five out of seven elements cannot be explained by core formation, and are much lower than the mantle estimates. These misfits might indicate that Bi, Cd, Sn, Zn, and In were added late, after core formation. (Color figure can be viewed at wileyonlinelibrary.com.)

(DeBaille et al., 2008; Righter and Chabot 2011; Yang et al. 2015). Using the same conditions for metal-silicate equilibrium as these previous studies (14 GPa, 2473 K, $\Delta IW = -1.25$ and core with 11 wt% S and 1 wt% C; e.g., Longhi et al. 1992; Righter and Chabot 2011; Rai and van Westrenen 2013; Yang et al. 2015), we can calculate the concentrations resulting in the Martian mantle. Comparison of the calculated to the mantle estimates from Righter et al. (2018a, 2018b) and Taylor (2013) shows a good match (Fig. 9b), suggesting that most of the volatile elements can be explained by a combination of volatile-depleted precursor materials and core formation. Even if Mars had a S-poor core, as suggested by Wang and Becker (2017) (e.g., Fig. 9b with 1 wt% S in the core), the mantle Bi content is still reproduced within error of the calculations. Future and more extensive studies of the chalcophile elements Bi and Ag at Mars interior conditions could be combined with new constraints on core size and composition provided by the InSight mission (Panning et al. 2017).

Vesta

Previous studies of Vesta's differentiation have suggested that Vesta experienced an early magma ocean (0.1 GPa and 1873 K) event that established the very low moderately siderophile element concentrations of Ni, Co, Mo, W, and P (Righter and Drake 1997; Holzheid and Palme 2007; Steenstra et al. 2016). Using the same conditions for metal-silicate equilibrium as these previous studies, we can calculate the VSE concentrations resulting in the vestan mantle. Comparison of the calculated to the mantle estimates from Righter et al. (2018a, 2018b) and this study (derived in supporting information Section 3: Table S3) shows a match only for P and Ag. Every other element —Bi, Zn, Sn, Cd, and In—is higher than expected after core formation (Fig. 9c). Consideration of S-poor and S-rich vestan core also does not influence this fundamental pattern; we have modeled both a 15 wt% S core and a 0.5 wt% S core, the latter derived from S contents in eucrites measured by Wu et al. (2018) and assuming sulfide undersaturation for the eucritic liquids. This mismatch suggests either that the volatile depletions have been overestimated, or that most VSE were added to the vestan mantle after core formation. Concentrations of most VSE may have been influenced by post core formation accretion, as also proposed for the HSEs in HEDs (Day et al. 2012). Post core formation accretion may also have delivered water and other highly volatile elements to Vesta, such as water and fluorine (Sarafian et al. 2017, 2018).

Even though late accretion may have altered the mantle concentrations of VSE, the core compositions should reflect the early metal-silicate equilibrium. Because our modeling also includes core concentrations, we can compare the calculated core concentrations to measurements of various VSE made on iron meteorites.

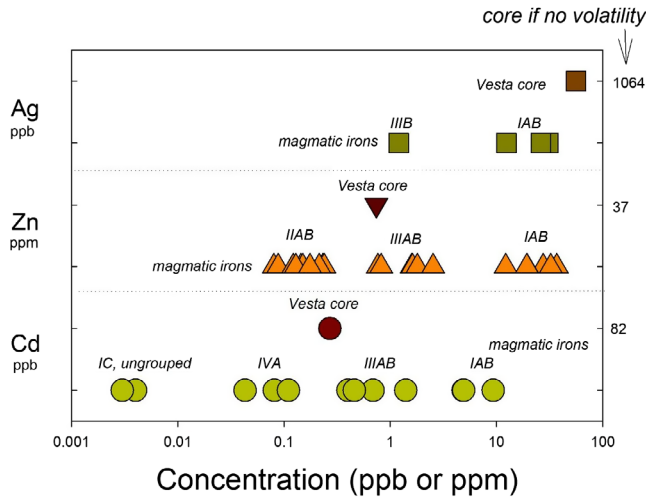

Fig. 10. Comparison of Ag, Zn, and Cd concentration measured in iron meteorites (from Woodland et al. 2005; Bridgestock et al. 2014; Kruijer et al. 2013, respectively) to the values calculated for Vesta's core in the siderophile element modeling. Also shown at the right edge of diagram are values expected in Vesta's core if the precursors were not volatile depleted. (Color figure can be viewed at wileyonlinelibrary.com.)

Kruijer et al. (2013), Bridgestock et al. (2014), and Woodland et al. (2005) measured Cd, Zn, and Ag in magmatic iron meteorites. Comparison of our calculated core concentrations and the measured values shows that for all three elements, the calculated core composition falls within the range of the magmatic iron groups (Fig. 10). Because the magmatic irons are ancient and record ages just a few million years after T_0, the Cd data indicate that these early planetesimals were already volatile depleted. Our works support the notion that the precursor materials for Vesta were volatile depleted and that the depletion occurred before accretion of the planetesimals. Otherwise, the core of Vesta would be expected to contain much higher levels of Cd, Zn, and Ag (Fig. 10).

CONCLUSIONS

Our results show that Si causes a substantial decrease in the metal-silicate partition coefficient, with the largest effect for P, and decreasing thereafter for Bi, Sn, Ag, and Cd. As a result, the Si content of the metal must be stipulated in any core formation model for a differentiated body. Even small amounts of Si cause 10× increase of the activity coefficient of P in Fe metal. The effect of Si on activity coefficients has been quantified using the epsilon interaction parameter model. Such large interaction coefficients for Fe-Si-S liquids will effectively cancel chalcophile activity that is expected in Fe-S liquids. Combination of these new results with existing interaction coefficient data allows the construction of a new model that includes Bi, Ag, Sn, and Cd.

Application of the model to various differentiated bodies reveals that most VSE in Earth and Mars mantles can be reconciled with core formation and precursor volatile loss. Bi and Ag are difficult to explain in Earth and Mars, which may indicate that the late segregation of sulfide is necessary to establish their contents. However, future efforts should also examine the pressure effect on activity coefficients and confirm pressure effects for metal/silicate partitioning, especially for Earth where extrapolation to higher pressure conditions is still required in the modeling. Mantle concentrations in Vesta are mostly inconsistent with volatile-depleted precursor materials combined with core formation (except for P) are present in higher concentrations than expected. This might be due to the effects of late accretion, as has been argued for the HSEs in some HEDs. Moreover, several VSE—Ag, Zn, and Cd—have modeled Vesta core concentrations that overlap with those of most magmatic iron meteorite groups, consistent with these volatile elements being depleted in the precursor material for Vesta.

Acknowledgements—This work was supported by RTOPs to K. R. from the NASA Cosmochemistry and LASER programs. Discussions with M Humayun and H. Becker were beneficial to the interpretations presented here.

Editorial Handling—Dr. Akira Yamaguchi

REFERENCES

Andrault D., Bolfan-Casanova N., Nigro G. L., Bouhifd M. A., Garbarino G., and Mezouar M. 2011. Solidus and liquidus profiles of chondritic mantle: Implication for melting of the Earth across its history. *Earth and Planetary Science Letters* 304:251–259.

Badro J., Fiquet G., Guyot F., Gregoryanz E., Occelli F., Antonangeli D., and d'Astuto M. 2007. Effect of light elements on the sound velocities in solid iron: Implications for the composition of Earth's core. *Earth and Planetary Science Letters* 254:233–238.

Ballhaus C., Fonseca R. O., Münker C., Rohrbach A., Nagel T., Speelmanns I. M., and Heuser A. 2017. The great sulfur depletion of Earth's mantle is not a signature of mantle–core equilibration. *Contributions to Mineralogy and Petrology* 172:68–80.

Barnes J. J., Tartese R., Anand M., McCubbin F. M., Neal C. R., and Franchi I. A. 2016. Early degassing of lunar urKREEP by crust-breaching impact(s). *Earth and Planetary Science Letters* 447:84–94.

Boesenberg J. S. and Delaney J. S. 1997. A model composition of the basaltic achondrite planetoid. *Geochimica et Cosmochimica Acta* 61:3205–3225.

Bridgestock L. J., Williams H., Rehkämper M., Larner F., Giscard M. D., Hammond S., and Smith C. L. 2014. Unlocking the zinc isotope systematics of iron meteorites. *Earth and Planetary Science Letters* 400:153–164.

Capobianco C. J., Drake M. J., and de'Aro J. 1999. Siderophile geochemistry of Ga, Ge, and Sn: Cationic oxidation states in silicate melts and the effect of composition in iron–nickel alloys. *Geochimica et Cosmochimica Acta* 63:2667–2677.

Chabot N. L., Safko T. M., and McDonough W. F. 2010. Effect of silicon on trace element partitioning in iron-bearing metallic melts. *Meteoritics & Planetary Science* 45:1243–1257.

Chang L., Malhotra S., and Schlesinger M. E. 1998. Thermodynamic properties of alumina-saturated iron-carbon-bismuth alloys. *Steel Research* 69:360–364.

Cleverly W. H., Jarosewich E., and Mason B. 1986. Camel Donga meteorite, a new eucrite from the Nullarbor Plain, Western Australia. *Meteoritics & Planetary Science* 21:263–269.

Day J. M., Walker R. J., Qin L., and Rumble D. III. 2012. Late accretion as a natural consequence of planetary growth. *Nature Geoscience* 5:614–620.

Debaille V., Yin Q. Z., Brandon A. D., and Jacobsen B. 2008. Martian mantle mineralogy investigated by the ^{176}Lu–^{176}Hf and ^{147}Sm–^{143}Nd systematics of shergottites. *Earth and Planetary Science Letters* 269:186–199.

De Laeter J. R., McCulloch M. T., and Rosman K. J. R. 1974. Mass spectrometric isotope dilution analyses of tin in stony meteorites and standard rocks. *Earth and Planetary Science Letters* 22:226–232.

Hertogen J., Janssens M. J., and Palme H. 1980. Trace elements in ocean ridge basalt glasses: Implications for fractionations during mantle evolution and petrogenesis. *Geochimica et Cosmochimica Acta* 44:2125–2143.

Hirose K., Labrosse S., and Hernlund J. 2013. Composition and state of the core. *Annual Review of Earth and Planetary Sciences* 41:657–691.

Holzheid A. and Palme H. 2007. The formation of eucrites: Constraints from metal-silicate partition coefficients. *Meteoritics & Planetary Science* 42:1817–1829.

Holzheid A., Palme H., and Chakraborty S. 1997. The activities of NiO, CoO and FeO in silicate melts. *Chemical Geology* 139:21–38.

Johnson A. and Canil D. 2011. The degassing behavior of Au, Tl, As, Pb, Re, Cd and Bi from silicate liquids: Experiments and applications. *Geochimica et Cosmochimica Acta* 75:1773–1784.

Jones J. H. and Drake M. J. 1986. Geochemical constraints on core formation in the Earth. *Nature* 322:221–228.

Kendall J. D. and Melosh H. J. 2016. Differentiated planetesimal impacts into a terrestrial magma ocean: Fate of the iron core. *Earth and Planetary Science Letters* 448:24–33.

Kiesl W., Weinke H. H., and Wichtl M. 1978. The Medanitos meteorite. *Meteoritics* 13:513–520.

Kiseeva E. S. and Wood B. J. 2013. A simple model for chalcophile element partitioning between sulphide and silicate liquids with geochemical applications. *Earth and Planetary Science Letters* 383:68–81.

Kitts K. and Lodders K. 1998. Survey and evaluation of eucrite bulk compositions. *Meteoritics & Planetary Science* 33:A197–A213.

Kruijer T. S., Sprung P., Kleine T., Leya I., and Wieler R. 2013. The abundance and isotopic composition of Cd in iron meteorites. *Meteoritics & Planetary Science* 48:2597–2607.

Laul J. C., Keays R. R., Ganapathy R., Anders E., and Morgan J. W. 1972. Chemical fractionations in meteorites —V. Volatile and siderophile elements in achondrites and ocean ridge basalts. *Geochimica et Cosmochimica Acta* 36:329–345.

Laurenz V., Rubie D. C., Frost D. J., and Vogel A. K. 2016. The importance of sulfur for the behavior of highly-siderophile elements during Earth's differentiation. *Geochimica et Cosmochimica Acta* 194:123–138.

Li Y. and Audétat A. 2012. Partitioning of V, Mn Co, Ni, Cu, Zn, As, Mo, Ag, Sn, Sb, W, Au, Pb, and Bi between sulfide phases and hydrous basanite melt at upper mantle conditions. *Earth and Planetary Science Letters* 355:327–340.

Li Y. and Audétat A. 2015. Effects of temperature, silicate melt composition, and oxygen fugacity on the partitioning of V, Mn Co, Ni, Cu, Zn, As, Mo, Ag, Sn, Sb, W, Au, Pb, and Bi between sulfide phases and silicate melt. *Geochimica et Cosmochimica Acta* 162:25–45.

Lin J. F., Campbell A. J., Heinz D. L., and Shen G. 2003. Static compression of iron-silicon alloys: Implications for silicon in the Earth's core. *Journal of Geophysical Research: Solid Earth* 108:2045. https://doi.org/10.1029/2002JB001978.

Liu J., Lin J.-F., Prakapenka V. B., Prescher C., and Yoshino T. 2016. Phase relations of Fe3C and Fe7C3 up to 185 GPa and 5200 K: Implication for the stability of iron carbide in the Earth's core. *Geophysical Research Letters* 43:12,415–12,422. https://doi.org/10.1002/2016GL071353

Lodders K. 2003. Solar system abundances and condensation temperatures of the elements. *The Astrophysical Journal* 591:1220–1248.

Lodders K. and Fegley B. 1997. An oxygen isotope model for the composition of Mars. *Icarus* 126:373–394.

Longhi J., Knittle E., and Holloway J. R. 1992. The bulk composition, mineralogy and internal structure of Mars. In *Mars*, vol. 20, edited by Kieffer H. H., Jakosky B. M., Snyder C. W., and Matthews M. Tucson, Arizona: University Arizona Press. pp. 184–208.

Loss R. D., Rosman K. J. R., and De Laeter J. R. 1990. The isotopic composition of zinc, palladium, silver, cadmium, tin, and tellurium in acid-etched residues of the Allende meteorite. *Geochimica et Cosmochimica Acta* 54:3525–3536.

Lupis C. H. 1983. *Chemical thermodynamics of materials*. New York City, New York: Elsevier Science Publishing Co., Inc. 581 p.

Ma Z. 2001. Thermodynamic description for concentrated metallic solutions using interaction parameters. *Metallurgical and Materials Transactions B* 32:87–103.

MacKenzie J. M. and Canil D. 2008. Volatile heavy metal mobility in silicate liquids: Implications for volcanic degassing and eruption prediction. *Earth and Planetary Science Letters* 269:488–496.

Mao Z., Lin J. F., Liu J., Alatas A., Gao L., Zhao J., and Mao H. K. 2012. Sound velocities of Fe and Fe-Si alloy in the Earth's core. *Proceedings of the National Academy of Sciences* 109:10,239–10,244.

McCubbin F. M., Kaaden K. E. V., Tartèse R., Klima R. L., Liu Y., Mortimer J., and Elardo S. M. 2015. Magmatic volatiles (H, C, N, F, S, Cl) in the lunar mantle, crust, and regolith: Abundances, distributions, processes, and reservoirs. *American Mineralogist* 100:1668–1707.

Mittlefehldt D. W. 2015. Asteroid (4) Vesta: I. The howardite-eucrite-diogenite (HED) clan of meteorites. *Chemie der Erde-Geochemistry* 75:155–183.

Morgan J. W., Higuchi H., Takahashi H., and Hertogen J. 1978. A "chondritic" eucrite parent body: Inference from trace elements. *Geochimica et Cosmochimica Acta* 42:27–38.

Morgan J. W., Wandless G. A., Petrie R. K., and Irving A. J. 1980. Composition of the Earth's upper mantle. II-Volatile trace elements in ultramafic xenoliths. Proceedings, 11th Lunar and Planetary Science Conference. pp. 213–233.

Norman M. D., Garcia M. O., and Bennett V. C. 2004. Rhenium and chalcophile elements in basaltic glasses from Ko'olau and Moloka'i volcanoes: Magmatic outgassing and composition of the Hawaiian plume. *Geochimica et Cosmochimica Acta* 68:3761–3777.

Norris C. A. and Wood B. J. 2017. Earth's volatile contents established by melting and vaporization. *Nature* 549:507–510.

O'Neill H. S. C. 1991. The origin of the Moon and the early history of the Earth—A chemical model. Part 2: The Earth. *Geochimica et Cosmochimica Acta* 55:1159–1172.

Palme H. and O'Neill H. 2014. Cosmochemical estimates of mantle composition. In *Planets, asteroids, comets and the solar system*, edited by Davis A. M. Treatise on Geochemistry, vol. 2. Heidelberg, Germany: Springer. pp. 1–39.

Paniello R. C., Day J. M., and Moynier F. 2012. Zinc isotopic evidence for the origin of the Moon. *Nature* 490:376–379.

Panning M. P., Lognonné P., Banerdt W. B., Garcia R., Golombek M., Kedar S., and Weber R. 2017. Planned products of the Mars structure service for the InSight mission to Mars. *Space Science Reviews* 211:611–650.

Paul R. L. and Lipschutz M. E. 1990. Chemical studies of differentiated meteorites: I. Labile trace elements in Antarctic and non-Antarctic eucrites. *Geochimica et Cosmochimica Acta* 54:3185–3196.

Rai N. and van Westrenen W. 2013. Core-mantle differentiation in Mars. *Journal of Geophysical Research: Planets* 118:1195–1203.

Righter K. 2011. Prediction of metal–silicate partition coefficients for siderophile elements: An update and assessment of PT conditions for metal–silicate equilibrium during accretion of the Earth. *Earth and Planetary Science Letters* 304:158–167.

Righter K. and Chabot N. L. 2011. Moderately and slightly siderophile element constraints on the depth and extent of melting in early Mars. *Meteoritics & Planetary Science* 46:157–176.

Righter K. and Drake M. J. 1997. A magma ocean on Vesta: Core formation and petrogenesis of eucrites and diogenites. *Meteoritics & Planetary Science* 32:929–944.

Righter K. and Drake M. J. 1999. Effect of water on metal-silicate partitioning of siderophile elements: A high pressure and temperature terrestrial magma ocean and core formation. *Earth and Planetary Science Letters* 171:383–399.

Righter K. and Drake M. J. 2000. Metal/silicate equilibrium in the early Earth—New constraints from the volatile moderately siderophile elements Ga, Cu, P, and Sn. *Geochimica et Cosmochimica Acta* 64:3581–3597.

Righter K., Drake M. J., and Yaxley G. 1997. Prediction of siderophile element metal-silicate partition coefficients to 20 GPa and 2800°C: The effects of pressure, temperature, oxygen fugacity, and silicate and metallic melt compositions. *Physics of the Earth and Planetary Interiors* 100:115–134.

Righter K., Humayun M., and Danielson L. 2008a. Partitioning of palladium at high pressures and temperatures during core formation. *Nature Geoscience* 1:321–323.

Righter K., Chesley J. T., Caiazza C. M., Gibson E. K., and Ruiz J. 2008b. Re and Os concentrations in arc basalts: The roles of volatility and source region fO_2 variations. *Geochimica et Cosmochimica Acta* 72:926–947.

Righter K., Pando K. M., Danielson L., and Lee C. T. 2010. Partitioning of Mo, P and other siderophile elements (Cu, Ga, Sn, Ni, Co, Cr, Mn, V, and W) between metal and silicate melt as a function of temperature and silicate melt composition. *Earth and Planetary Science Letters* 291:1–9.

Righter K., King C., Danielson L., Pando K., and Lee C. T. 2011. Experimental determination of the metal/silicate partition coefficient of Germanium: Implications for core and mantle differentiation. *Earth and Planetary Science Letters* 304:379–388.

Righter K., Danielson L. R., Pando K. M., Williams J., Humayun M., Hervig R. L., and Sharp T. G. 2015. Highly siderophile element (HSE) abundances in the mantle of Mars are due to core formation at high pressure and temperature. *Meteoritics & Planetary Science* 50:604–631.

Righter K., Danielson L. R., Pando K. M., Shofner G. A., Sutton S. R., Newville M., and Lee C. T. 2016. Valence and metal/silicate partitioning of Mo: Implications for conditions of Earth accretion and core formation. *Earth and Planetary Science Letters* 437:89–100.

Righter K., Nickodem K., Pando K., Danielson L., Boujibar A., Righter M., and Lapen T. J. 2017a. Distribution of Sb, As, Ge, and In between metal and silicate during accretion and core formation in the Earth. *Geochimica et Cosmochimica Acta* 198:1–16.

Righter K., Pando K., and Ross D. K. 2017b. Effect of silicon on activity coefficients of P, Bi, Cd, Sn, and Ag in liquid Fe-Si, and implications for differentiation and core formation. Annual Meeting of The Meteoritical Society; 80th; 23–28 July 2017; Santa Fe, New Mexico, USA.

Righter K., Pando K., Marin N., Ross D. K., Righter M., Danielson L., and Lee C. 2018a. Volatile element signatures in the mantles of Earth, Moon, and Mars: Core formation fingerprints from Bi, Cd, In, and Sn. *Meteoritics & Planetary Science* 52:284–305.

Righter K., Pando K., Humayun M., Waeselmann N., Yang S., Boujibar A., and Danielson L. R. 2018b. Effect of silicon on activity coefficients of siderophile elements (Au, Pd, Pt, P, Ga, Cu, Zn, and Pb) in liquid Fe: Roles of core formation, late sulfide matte, and Late veneer in shaping terrestrial mantle geochemistry. *Geochimica et Cosmochimica Acta* 232:101–123.

Righter K., Pando K., Rowland R., Ross D. K., Righter M., and Lapen T. J. 2019. Core-mantle partitioning of Silver and Bismuth from 0 to 20 GPa, with application to core formation in Earth and Mars (abstract #1104). 50th Lunar and Planetary Science Conference. CD-ROM.

Robie R. A., Hemingway B. S., and Fisher J. R. 1978. Thermodynamic properties of minerals and related substances at 298.15 K and 1 bar (10^5 Pascal) pressure and at higher temperatures. *Bulletin of the United States Geological Survey* 1452:456.

Rubie D. C., Laurenz V., Jacobson S. A., Morbidelli A., Palme H., Vogel A. K., and Frost D. J. 2016. Highly siderophile elements were stripped from Earth's mantle by iron sulfide segregation. *Science* 353:1141–1144.

Rubin K. 1997. Degassing of metals and metalloids from erupting seamount and mid-ocean ridge volcanoes: Observations and predictions. *Geochimica et Cosmochimica Acta* 61:3525–3542.

Sanloup C., Fiquet G., Gregoryanz E., Morard G., and Mezouar M. 2004. Effect of Si on liquid Fe compressibility: Implications for sound velocity in core materials. *Geophysical Research Letters* 31:L07604. https://doi.org/10.1029/2004GL019526

Sarafian A. R., John T., Roszjar J., and Whitehouse M. J. 2017. Chlorine and hydrogen degassing in Vesta's magma ocean. *Earth and Planetary Science Letters* 459:311–319.

Sarafian A. R., Nielsen S. G., Marschall H. R., Hauri E. H., Gaetani G. A., Righter K., Grove T. L., and Berger E. L. 2018. The water and fluorine content of 4 Vesta. *Geochimica et Cosmochimica Acta*. In press.

Schönbächler M., Carlson R. W., Horan M. F., Mock T. D., and Hauri E. H. 2010. Heterogeneous accretion and the moderately volatile element budget of Earth. *Science* 328:884–887.

Siebert J., Corgne A., and Ryerson F. J. 2011. Systematics of metal–silicate partitioning for many siderophile elements applied to Earth's core formation. *Geochimica et Cosmochimica Acta* 75:1451–1489.

Smith M. R., Laul J. C., Ma M. S., Huston T., Verkouteren R. M., Lipschutz M. E., and Schmitt R. A. 1984. Petrogenesis of the SNC (shergottites, nakhlites, chassignites) meteorites: Implications for their origin from a large dynamic planet, possibly Mars. *Journal of Geophysical Research: Solid Earth* 89:612–630.

Steelmaking Data Sourcebook. 1988. *The 19th committee on steelmaking*. Montreux, Switzerland: JSPS, Gordon and Breach Science Publishers. 59 p.

Steenstra E. S., Knibbe J. S., Rai N., and Van Westrenen W. 2016. Constraints on core formation in Vesta from metal–silicate partitioning of siderophile elements. *Geochimica et Cosmochimica Acta* 177:48–61.

Taylor G. J. 2013. The bulk composition of Mars. *Chemie Der Erde-Geochemistry* 73:401–420.

Treiman A. H., Drake M. J., Janssens M. J., Wolf R., and Ebihara M. 1986. Core formation in the Earth and shergottite parent body (SPB): Chemical evidence from basalts. *Geochimica et Cosmochimica Acta* 50:1071–1091.

Tuff J., Wood B. J., and Wade J. 2011. The effect of Si on metal–silicate partitioning of siderophile elements and implications for the conditions of core formation. *Geochimica et Cosmochimica Acta* 75:673–690.

Vogel A. K., Jennings E. S., Laurenz V., Rubie D. C., and Frost D. J. 2018. The dependence of metal-silicate partitioning of moderately volatile elements on oxygen fugacity and Si contents of Fe metal: Implications for their valence states in silicate liquids. *Geochimica et Cosmochimica Acta* 237:275–293.

Wade J. and Wood B. J. 2005. Core formation and the oxidation state of the Earth. *Earth and Planetary Science Letters* 236:78–95.

Wang Z. and Becker H. 2017. Silver contents and Cu/Ag ratios in Martian meteorites and the implications for planetary differentiation. *Geochimica et Cosmochimica Acta* 216:96–113.

Wang Z., Laurenz V., Petitgirard S., and Becker H. 2016. Earth's moderately volatile element composition may not be chondritic: Evidence from In, Cd and Zn. *Earth and Planetary Science Letters* 435:136–146.

Wanke H. and Dreibus G. 1986. Geochemical evidence for the formation of the Moon by impact-induced fission of the proto-Earth. In *Origin of the Moon*, edited by Hartmann W., Phillips R. J., and Taylor G. J. Houston, Texas: Lunar and Planetary Institute. pp. 649–682.

Wasson J. T. 1985. *Meteorites: Their record of early solar-system history*. New York: WH Freeman and Co. 274 p.

Wheeler K. T., Walker D., and McDonough W. F. 2011. Pd and Ag metal-silicate partitioning applied to Earth differentiation and core-mantle exchange. *Meteoritics & Planetary Science* 46:199–217.

Wolf R., Woodrow A., and Anders E. 1979. Lunar basalts and pristine highland rocks-Comparison of siderophile and volatile elements. Proceedings, 10th Lunar and Planetary Science Conference. pp. 2107–2130.

Wombacher F., Rehkämper M., Mezger K., and Münker C. 2003. Stable isotope compositions of cadmium in geological materials and meteorites determined by multiple-collector ICPMS. *Geochimica et Cosmochimica Acta* 67:4639–4654.

Wombacher F., Rehkämper M., Mezger K., Bischoff A., and Münker C. 2008. Cadmium stable isotope cosmochemistry. *Geochimica et Cosmochimica Acta* 72:646–667.

Wood B. J., Walter M. J., and Wade J. 2006. Accretion of the Earth and segregation of its core. *Nature* 441:825–827.

Wood B. J., Kiseeva E. S., and Mirolo F. J. 2014. Accretion and core formation: The effects of sulfur on metal–silicate partition coefficients. *Geochimica et Cosmochimica Acta* 145:248–267.

Woodland S. J., Rehkämper M., Halliday A. N., Lee D. C., Hattendorf B., and Günther D. 2005. Accurate measurement of silver isotopic compositions in geological materials including low Pd/Ag meteorites. *Geochimica et Cosmochimica Acta* 69:2153–2163.

Wu N., Farquhar J., Dottin J. W., and Magalhães N. 2018. Sulfur isotope signatures of eucrites and diogenites. *Geochimica et Cosmochimica Acta* 233:1–13.

Yang S., Humayun M., Righter K., Jefferson G., Fields D., and Irving A. J. 2015. Siderophile and chalcophile element abundances in shergottites: Implications for Martian core formation. *Meteoritics & Planetary Science* 50:691–714.

SUPPORTING INFORMATION

Additional supporting information may be found in the online version of this article:

Data S1. Sections 1–6.